

LETTER • OPEN ACCESS

Flux-pinning mediated superconducting diode effect in NbSe₂/CrGeTe₃ heterostructure

To cite this article: A Mehrnejat *et al* 2024 *2D Mater.* **11** 021002

View the [article online](#) for updates and enhancements.

You may also like

- [High Curie temperature and strain-induced semiconductor-metal transition with spin reorientation transition in 2D CrPbTe₃ monolayer](#)
Imran Khan and Jisang Hong
- [Emerging intrinsic magnetism in two-dimensional materials: theory and applications](#)
Songrui Wei, Xiaoqi Liao, Cong Wang et al.
- [Recent progress of spintronics based on emerging 2D materials: CrI₃ and Xenes](#)
Songrui Wei, Xian Tang, Xiaoqi Liao et al.



LETTER

OPEN ACCESS

RECEIVED
18 October 2023REVISED
26 December 2023ACCEPTED FOR PUBLICATION
9 February 2024PUBLISHED
22 February 2024

Original content from
this work may be used
under the terms of the
[Creative Commons
Attribution 4.0 licence](#).

Any further distribution
of this work must
maintain attribution to
the author(s) and the title
of the work, journal
citation and DOI.



Flux-pinning mediated superconducting diode effect in NbSe₂/CrGeTe₃ heterostructure

A Mehrnejat^{1,*}, M Ciomaga Hatnean² , M C Rosamond³, N Banerjee^{1,4} , G Balakrishnan² ,
S E Savel'ev¹ and F K Dejene^{1,*}

¹ Department of Physics, Loughborough University, Loughborough LE11 3TU, United Kingdom

² Department of Physics, University of Warwick, Coventry CV4 7AL, United Kingdom

³ School of Electronic and Electrical Engineering, University of Leeds, Leeds LS2 9JT, United Kingdom

⁴ Department of Physics, Blackett Laboratory, Imperial College London, London SW7 2AZ, United Kingdom

* Authors to whom any correspondence should be addressed.

E-mail: a.mehrnejat@lboro.ac.uk and f.dejene@lboro.ac.uk

Keywords: flux-pinning, NbSe₂/CrGeTe₃, NbSe₂, CrGeTe₃, superconducting diode effect, superconducting spintronics, van der Waals heterostructure

Abstract

In ferromagnet/superconductor bilayer systems, dipolar fields from the ferromagnet can create asymmetric energy barriers for the formation and dynamics of vortices through flux pinning. Conversely, the flux emanating from vortices can pin the domain walls of the ferromagnet, thereby creating asymmetric critical currents. Here, we report the observation of a superconducting diode effect (SDE) in a NbSe₂/CrGeTe₃ van der Waals heterostructure in which the magnetic domains of CrGeTe₃ control the Abrikosov vortex dynamics in NbSe₂. In addition to extrinsic vortex pinning mechanisms at the edges of NbSe₂, flux-pinning-induced bulk pinning of vortices can alter the critical current. This asymmetry can thus be explained by considering the combined effect of this bulk pinning mechanism along with the vortex tilting induced by the Lorentz force from the transport current in the NbSe₂/CrGeTe₃ heterostructure. We also provide evidence of critical current modulation by flux pinning depending on the history of the field setting procedure. Our results suggest a method of controlling the efficiency of the SDE in magnetically coupled van der Waals superconductors, where dipolar fields generated by the magnetic layer can be used to modulate the dynamics of the superconducting vortices in the superconductors.

1. Introduction

Type II superconductors (type II SCs) are distinguished by their characteristic mixed state in the phase diagram due to the appearance of superconducting vortices [1]. The dynamics of these Abrikosov vortices can be modified by applied current, external magnetic field, sample geometry/confinement [2, 3], and magnetic proximity effect [4–6], thereby opening various possibilities for controlling device properties, for instance, the superconducting diode effect (SDE) [7–9]. The appearance of nonreciprocal current-voltage characteristics in a superconductor has received revived interest following the observation of field-free superconducting rectification effects in van der Waals heterostructures (vdWHs) and multilayered Rashba superconductors [10, 11]. These SDEs were reported to arise from breaking

inversion symmetry and time-reversal symmetry [12]. Asymmetric critical currents have also been observed in other works using conformally mapped nanoholes [13], size confinement in constrictions [2], and Josephson junctions [14, 15]. It is plausible that asymmetric I–V characteristics can arise from extrinsic properties such as interface or edge roughness in lithographically defined constrictions [16] or other intrinsic mechanisms such as asymmetric vortex-flow energy barriers [1, 17, 18], magnetic flux penetration [19, 20], flux pinning effects [21, 22], vortex limited critical currents [23] and avalanches [24, 25]. Hence, identifying the key driving mechanisms of the SDE and establishing their relations to other nonreciprocal transport effects is of paramount importance for future superconducting electronic as well as spintronic devices. Atomically flat interfaces in artificially engineered

vdWHs, which have been integral in the discovery of various emergent quantum effects in spintronic, thermoelectric, superconducting, and optical applications [26–28], could offer unique possibilities for a more detailed understanding of the mechanisms of SDEs by excluding extrinsic interfacial mixing or disorder.

In this work, we demonstrate the observation of SDE in the vdWHs of NbSe₂/CrGeTe₃ (CGT), where the magnetic domain walls in CGT offer a unique possibility for guiding superconducting vortices [29, 30] essential for magnetically controlled pinning of vortices at the NbSe₂/CGT interface [21]. NbSe₂ is an anisotropic layered superconductor extensively studied for its unique superconducting and spintronic properties in thicknesses down to the monolayer regime [2, 31–35]. CGT is a 2D magnetic semiconductor ($E_g \sim 0.38$ eV) [36] with a Curie temperature of approximately 65 K and exhibits diverse thickness-dependent magnetic domain transformations [37, 38]. The magnetic coupling of superconducting NbSe₂ with CGT allows us to exploit its topological vortex phase transitions by modifying the confinement potentials [39] of Abrikosov vortices and, in turn, controlling the SDE via asymmetric flux-pinning at the NbSe₂/CGT and NbSe₂/SiO₂ interfaces [23].

2. Methods

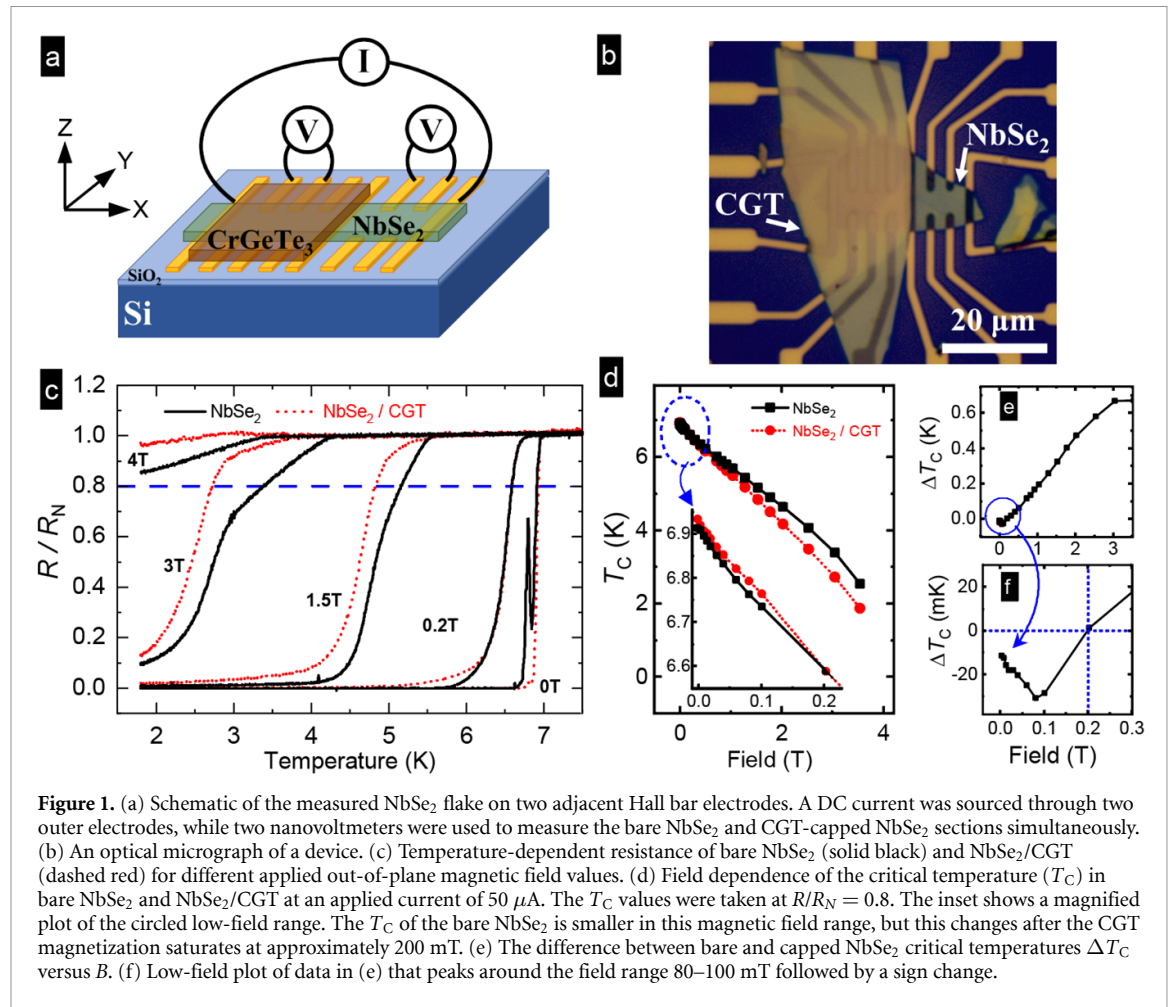
Figure 1(a) shows a schematic diagram of our NbSe₂/CGT vdWH device, along with the electrical configuration for longitudinal resistance measurement. The NbSe₂ crystals ($\geq 99.999\%$ purity) were obtained from Ossila Ltd. The CGT ($\geq 99.99\%$ purity) crystals were grown using the flux method as described in [40]. Figure 1(b) shows an example micrograph of one of the measured devices (named device B) comprising adjacent NbSe₂/CGT and bare NbSe₂ devices, which we measured at the same time under identical experimental conditions in a Cryogenic Ltd cryostat. We adopted a top-down device fabrication approach where the vdWH (NbSe₂/CGT) was transferred onto a pre-patterned Si/SiO₂ substrate with Ti/Au (45 nm) electrical contacts patterned using standard UV lithography and e-beam evaporation. In the first step of our device fabrication, NbSe₂ and CGT crystals were mechanically exfoliated onto two different polydimethylsiloxane stamps (from Teltec Ltd) under ambient conditions. After identifying homogenous flakes, we first transferred the NbSe₂ flake on the contacts, followed by the CGT flake transfer on one side of the NbSe₂ flake. We fabricated and studied several devices with NbSe₂ thicknesses ranging from 5 nm up to 45 nm, while

device degradation due to the oxidation of flakes was minimized by completing flake-transfer processes in under an hour.

3. Results

We performed temperature-dependent resistance measurements (RT) of both the bare and capped NbSe₂ sides. The current was applied along the x -direction (as shown in figure 1(a)) parallel to the ab -plane of NbSe₂, while an out-of-plane (OOP) external magnetic field was applied along the z -direction parallel to the c -axis of the flake. Figure 1(c) shows the RT of a device (labeled device A) for various applied magnetic fields. The zero-field critical temperature of the bare NbSe₂ ($T_C \sim 6.93$ K) is just slightly larger than the CGT-capped NbSe₂ critical temperature ($T_C \sim 6.91$ K); otherwise, both T_C values are close to that of bulk NbSe₂, indicating the high quality of our devices, as confirmed by the residual resistivity ratios [$RRR = R$ (room temperature)/ R (above T_C)] ranging from 10 to 20, typical for exfoliated NbSe₂ flakes [32, 35]. Figure 1(d) depicts the field dependence of the T_C extracted based on the 80% line of the normalized resistance plots in figure 1(c). Here, we can observe that for $B < 200$ mT, the critical temperature of NbSe₂/CGT is slightly higher than that of bare NbSe₂ (see the inset in figure 1(d)). On the other hand, when $B > 200$ mT and CGT is saturated, the T_C of the bare NbSe₂ is larger than that of the NbSe₂/CGT. This corresponds to the magnetization saturation field of the bulk CGT crystal (later shown in figure 4(c)). For the bare side, in the low-field range, the transition is accompanied by the appearance of intermediate kinks previously attributed to phase slips or inhomogeneous strain distribution [41, 42]. To illustrate this further, we plotted $\Delta T_C = T_C^{\text{NbSe}_2} - T_C^{\text{NbSe}_2/\text{CGT}}$ in figures 1(e) and (f), where a clear sign change of ΔT_C at $B = 200$ mT corresponds to the magnetization saturation point of CGT. It is also worth noting that for $\Delta T_C < 0$ values in figure 1(f), the minimum is located in the field range of 80–100 mT, which, as we show later, plays a major role in the modulation of the critical current via the magnetic domain reorientation of CGT or flux-pinning [38, 43].

Next, we present magnetoresistance (MR) measurements of our devices with an OOP external magnetic field (see figure 2(a)). The CGT/NbSe₂ MR curve exhibits hysteresis with different H_C values for trace and retrace measurements. This hysteretic MR feature, which is completely absent in the bare NbSe₂ flakes, can be attributed to flux pinning in NbSe₂ by the CGT domains [21] and corresponds to the field regime where a sign change in ΔT_C was observed in



figures 1(e) and (f). To identify the asymmetry in the trace and retrace H_C values, we define H_C^{tr1} (H_C^{tr2}) as the positive (negative) H_C value when sweeping the field from 0.5 T to -0.5 T, as shown in figure 2(a), where the solid curve represents the trace measurements. Similar parameters are defined on the retrace measurement (dashed curve) from -0.5 T to 0.5 T. When tracing/retracing the field from higher magnitudes toward 0 T, there is a sharp transition from the mixed state to the Meissner phase; however, the transition is smoother when increasing the field value from 0 T to higher magnitudes, indicative of stronger vortex pinning. To observe how these lower critical fields develop by increasing the applied current, we performed MR measurements for varying currents. The current dependence of $|H_C^{\text{tr2}}|$ and $|H_C^{\text{retr2}}|$, obtained from the extrema of the first field derivative of MR and plotted in figure 2(b), does not show an appreciable difference over the measured field range. Nevertheless, based on this observation and by comparing several I–V measurements collected in the flux-pinning window, we can estimate the strength of the pinned flux in NbSe₂. We consider a series of I–V measurements collected at 100 mT while the field is set to this value through two different scenarios: first, by coming from the higher field of +150 mT (solid black line in figure 2(c) noted as V_{HL}), and

second, by coming from the lower field of 0 T (dashed red line, V_{LH} for lower to higher). As shown in the inset here (adapted from figure 2(a)), one of these two I–V sweeps represents the Meissner phase, and the other is performed in the dissipative phase of the Abrikosov lattice inside the hysteretic flux-pinning regime. The observed opening between the two I–V curves arises at currents above 0.5 mA, which also agrees with the appearance of hysteresis in the MR measurements. We can estimate the amount of this trapped flux to be approximately 20 mT by observing the relative overlap of the I–V curve at an applied field of 120 mT, which was set to this value by coming from an initial 0 T (blue dashed line in figure 2(c)). Figure 2(d) depicts the difference between V_{HL} and V_{LH} , which shows how this difference changes the sign for field values inside and outside of this pinning window resulting from the modulation of the critical current (the inset shows the MR for another device).

After establishing the impact of the CGT magnetization on the superconductivity of NbSe₂, we next discuss the characterizations of the SDE in the NbSe₂/CGT heterostructure side of device B. This device comprises a thin NbSe₂ flake (5 nm) and exhibits smaller critical currents, as expected for thinner superconductors [44]. As such, we limited the

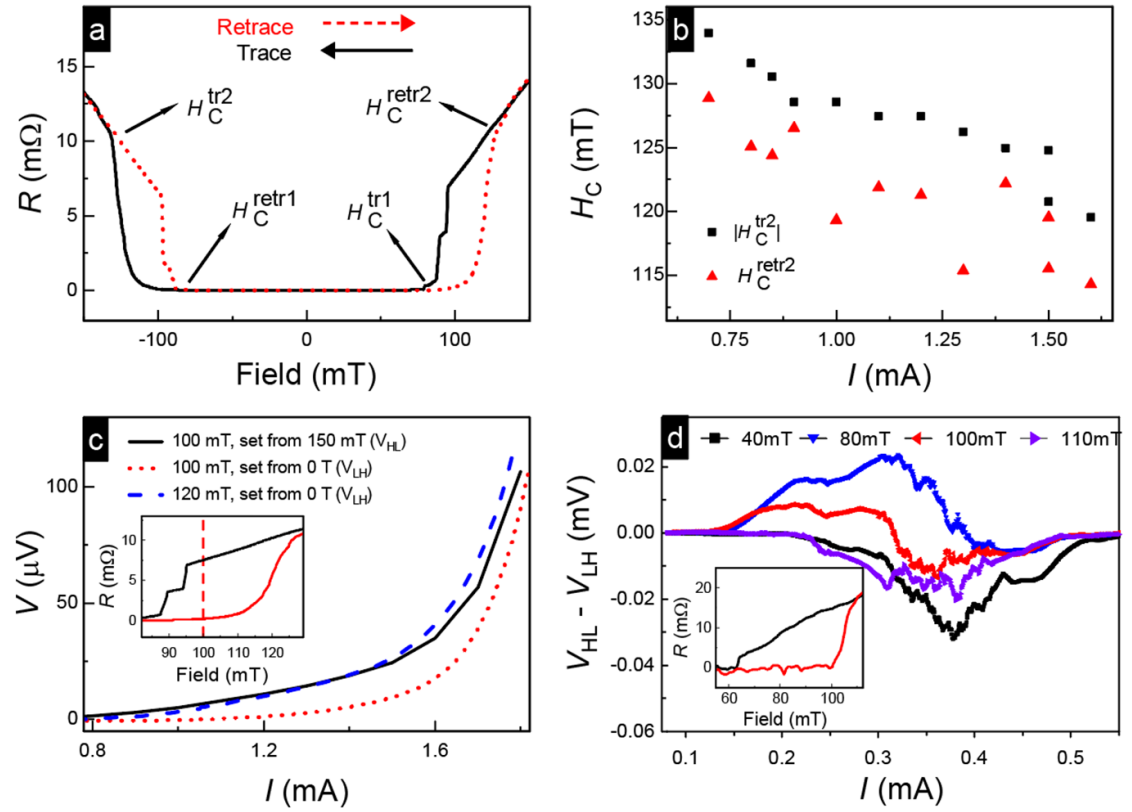
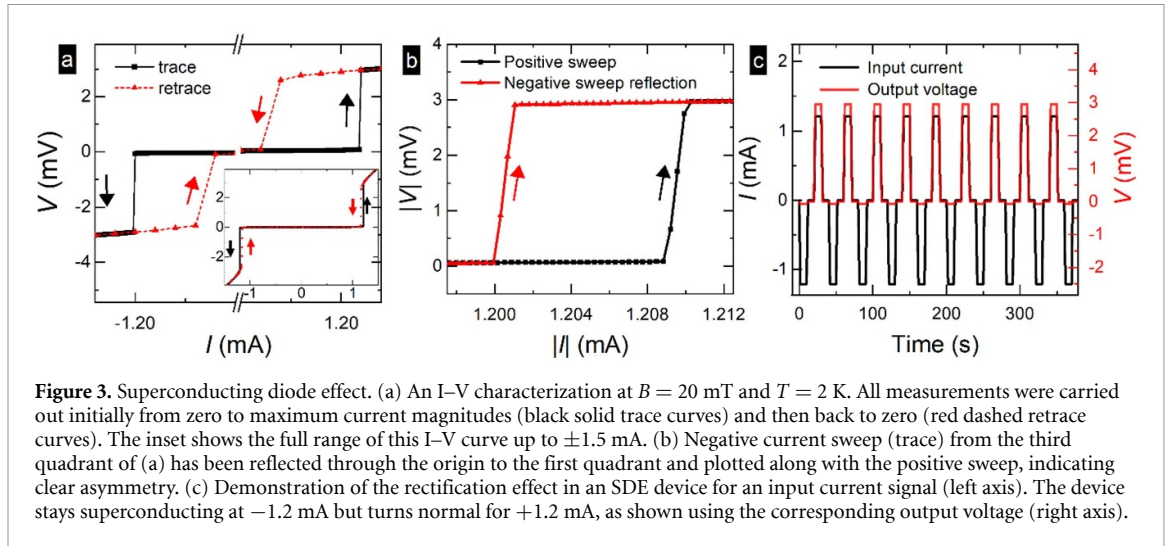


Figure 2. (a) Magnetoresistance measurements of NbSe₂/CGT showing hysteresis at 1 mA and 2 K. For traces (black) and retraces (dotted red), the definitions of lower critical fields are shown by arrows. (b) Comparison of $H_C^{\text{tr}2}$ and $|H_C^{\text{tr}2}|$ values as a function of the applied current showing a relatively identical trend. (c) Magnetic-field history dependence of the I-V curves at 100 mT (see inset) obtained by following the two field-setting scenarios V_{HL} (higher to lower field, solid black) and V_{LH} (lower to higher field, dotted red). The large dashed blue curve is the I-V data for an applied field of 120 mT (V_{LH}). The three I-V curves can be used to estimate a trapped flux of ~ 20 mT. (d) The difference $V_{\text{HL}} - V_{\text{LH}}$ between measured I-V curves for similar field-setting scenarios shown in (c) highlights the role of flux-pinning for 80 mT and 100 mT, as shown in the inset MR.

maximum applied current to below 2 mA to maintain high device quality and temperature-dependent stability. Figure 3(a) illustrates a typical trace and retrace I-V characterization of NbSe₂/CGT at an applied out-of-plane field of 20 mT. The trace curves (solid black) were recorded by sweeping current first from zero to the maximum positive current and second from zero to the maximum magnitude of the negative current. The retrace measurements (dashed red) from the maximum magnitudes back to 0 are not the focus of this paper but represent the retrapping current [9, 45]. The positive critical currents (here: $I_C^+ = 1208 \pm 1 \mu\text{A}$) and negative critical currents ($I_C^- = -1200 \pm 1 \mu\text{A}$) on positive and negative sweeps are different, indicating nonreciprocal transport of this SDE device with a nonreciprocity window of nearly $8 \mu\text{A}$. Figure 3(b) depicts this window more clearly through the reflection (through the origin) of the negative critical current to the first quadrant. As mentioned above, these two curves are derived from the trace measurements where the current has been swept from lower to higher current magnitudes; thus, heat dissipation processes are relatively identical. As a proof of concept for SDE, we show the device rectification

measurements in figure 3(c), in which the input signal is a current pulse with symmetric positive and negative values of approximately ± 1.2 mA that fit in the nonreciprocity window shown in figure 3(b), and the measured output voltage plotted with red dashed lines clearly demonstrates the rectifying behavior.

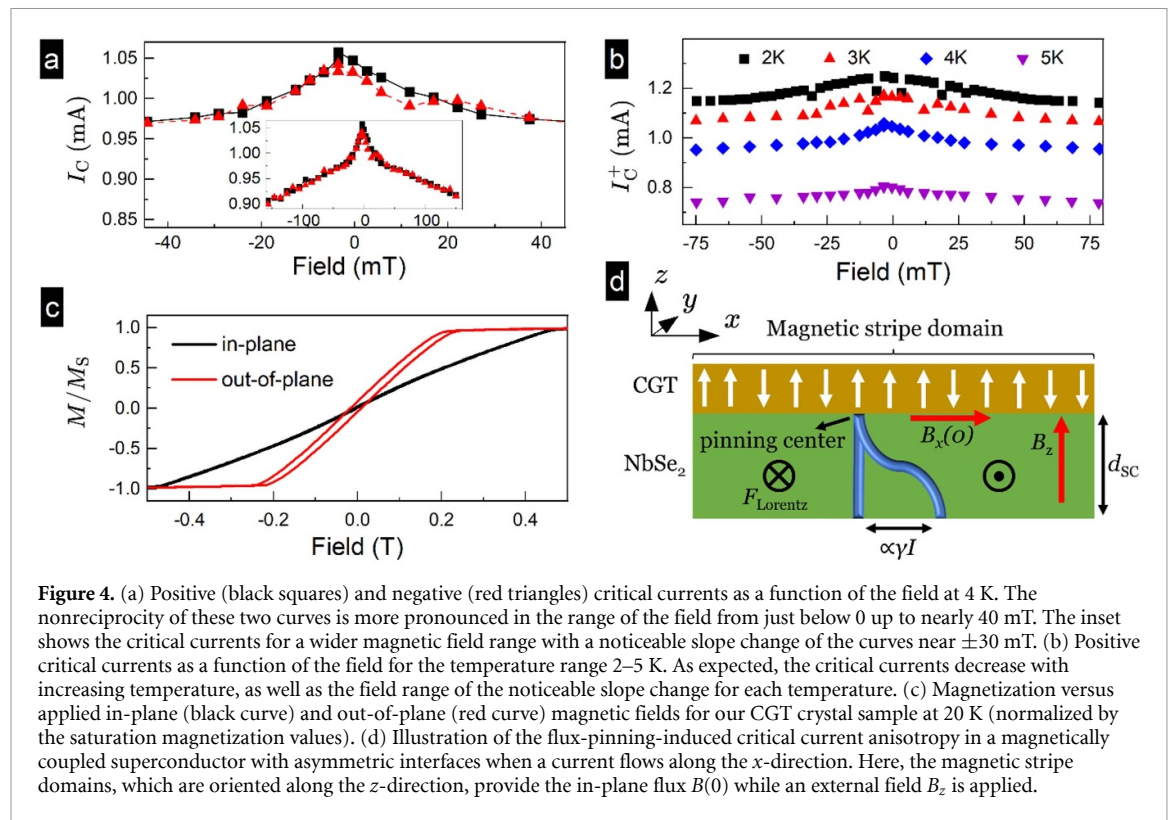
Figure 4(a) shows the dependence of the positive critical currents (I_C^+) and the absolute value of the negative critical currents (I_C^-) on the applied OOP magnetic field at 4 K. In this exemplary case, the nonreciprocity is especially pronounced for fields below 40 mT, with the inset showing a wider magnetic field range of ± 150 mT. We note a change in the overall slope of the resulting graph with the kinks at approximately ± 30 mT, which marks a transition between a fast and slow decay of I_C values. Figure 4(b) presents the positive critical currents of the heterostructure for different temperatures from 2 K to 5 K. With increasing temperature, we observe a decrease in the field range where the slope increases. In this figure, the corresponding negative critical currents are not depicted in the interest of distinguishing the plotted curves. It is also observed here that the maximum magnitude of the critical currents at each temperature



decreased from 1.25 mA at 2 K to 0.8 mA at 5 K. We note that our maximum rectification ratio ($Q \equiv 2(I_C^+ - |I_C^-|)/(I_C^+ + |I_C^-|)$) was $\sim 5\%$ observed at 2 K. In addition, we have also observed that the Q-factor shows oscillatory behavior at some data points, which can be attributed to CGT magnetic domain reorientation or phase transitions of the finite-momentum pairing states [46]. Figure 4(c) shows the magnetization measurement of our CGT crystal for magnetic fields applied parallel to the ab -plane (black curve) and c -axis (red curve). The magnetization measurement along the c -axis saturates at a lower field, suggesting an easy axis along this crystallographic direction.

When NbSe₂ is magnetically coupled to a CGT flake, dipolar fields from the CGT magnetic texture ($B < 50$ mT) can control the formation and dynamics of Abrikosov vortices in NbSe₂. Due to the asymmetric boundaries of NbSe₂, which is interfaced with CGT from one surface but with SiO₂ at the other surface, the forces at the vortex ends are not equal. This may cause a tilted core with stronger dynamics at the top NbSe₂/CGT interface than at the bottom NbSe₂/SiO₂. This asymmetry can be considered in explaining the nonreciprocal current-voltage characteristics [4]. As shown in figure 4(a), we have observed a similar asymmetry between the two curves, likely due to the CGT magnetic domains that have not yet fully aligned with the applied out-of-plane field. To shed more light on this pinning mechanism, we consider a simple bilayer structure (figure 4(d)) and estimate the critical-current asymmetry induced by magnetic domains. In the asymmetric magnetic environment, vortices are tilted, and their length can be estimated as $L = d_{SC} \sqrt{1 + B_x^2(0)/B_z^2}$, where d_{SC} is the thickness of the superconducting NbSe₂; B_z is the external

magnetic field; and $B_x(0)$ is the field component due to the asymmetric magnetic environment (dipolar field), which depends on the sweep direction of B_z and applied bias current I . Stray fields, which are generated by the stripe magnetic domains in the CGT, close inside the superconducting NbSe₂ flake thereby generating a non-zero in-plane field component $B_x(I = 0)$ at zero applied current I . The sign and magnitude of $B_x(0)$ is determined by the random distribution of domains and the imbalance between the number of up and down domains by the applied magnetic field along the z -axis. The Lorentz force is proportional to the applied current I and d_{SC} and can therefore be given as $F_L = \alpha d_{SC} I$. However, the pinning force is proportional to the number of pinning centers that can trap the vortex line. If the pinning centers are homogeneously distributed in the sample (no asymmetry) with an average distance of a between them, then the pinning force is $F_p = \beta L/a$. In F_L and F_p , α and β are the magnetic-field independent constants. In the presence of a bias current, the magnetic-environment field component B_x changes proportionally to the current as $B_x = B_x(0) + \gamma I$, where γ is a material-specific constant. The physical origin of the in-plane field $B_x(0)$ generated by the charge current occurs due to the requirement of Ampere's law: $I \sim \Delta B_z/d_{SC} - \Delta B_x/\delta_W$ with ΔB_z and ΔB_x being the changes in the out-of-plane and in-plane magnetic field components, respectively, while δ_W is the characteristic stripe domain wall width. By estimating the critical current I_C through the balance of the pinning force and Lorentz force at $I = I_C$, we obtain the equation $\alpha d_{SC} I_C = (\beta/a) d_{SC} \sqrt{1 + (B_x(0) + \gamma I_C)^2/B_z^2}$, whose solution is not symmetric under current reversal ($I_C^+ \neq I_C^-$). This simple explanation captures the observed asymmetry in an asymmetric magnetic



environment $B_x(0) \neq 0$ even if pinning centers are homogeneously distributed. To obtain a deeper phenomenological understanding of the SDE, combining the transport measurements (as in this work) with direct microscopic imaging of vortex dynamics will be useful to reveal the actual operation mechanism at play [47]. We also anticipate that employing additional constrictions of varying dimensions to exploit extrinsic pinning, as in [2], will offer pathways to further increase the Q -factors.

4. Conclusion

In conclusion, we have reported the observation of the SDE in a $\text{NbSe}_2/\text{CrGeTe}_3$ vdWH, where the size and asymmetry of the critical currents are modulated by the applied magnetic field, the magnetic domain texture of the CGT and inherent flux pinning in the $\text{NbSe}_2/\text{CrGeTe}_3$ heterostructure. Furthermore, this pinning effect, due to the asymmetric magnetic environments and magnetic domain transformations, can provide a means to tune and utilize the SDE for energy harvesting from ambient radiation. More studies are required to improve the rectification efficiency and relation between intrinsic and extrinsic pinning effects using nanofabricated $\text{NbSe}_2/\text{CrGeTe}_3$ devices with constrictions, for instance, by modifying the shape anisotropy of CGT as well as the critical

currents of NbSe_2 . It is also interesting to look at the effects of the CGT thickness on the rectification behavior since ultrathin CGT flakes (< 10 nm) exhibit very low demagnetization fields. Our results lay the groundwork for exploring the possibility of the field-programmable SDE and its manipulation through magnetic textures in two-dimensional systems.

Data availability statement

All data that support the findings of this study are included within the article (and any supplementary files).

Acknowledgments


We thank Akashdeep Kamra for the fruitful discussion. The research conducted at Loughborough University received support from the School of Science strategic fund and EPSRC, UK, through a Grant for multiuser equipment EP/P030599/1. We wish to acknowledge the support of the Henry Royce Institute for Advanced Materials for A M through the Student Equipment Access Scheme enabling access to the cleanroom facilities at the University of Leeds; EPSRC Grant Number EP/R00661X/1. The work at the University of Warwick was supported by EPSRC, UK, through Grants EP/T005963/1 and EP/N032128/1.


ORCID iDs

M Ciomaga Hatnean  <https://orcid.org/0000-0003-2870-8847>

N Banerjee  <https://orcid.org/0000-0002-2027-4434>

G Balakrishnan  <https://orcid.org/0000-0002-5890-1149>

S E Savel'ev  <https://orcid.org/0000-0003-2771-230X>

F K Dejene  <https://orcid.org/0000-0002-1605-8835>

References

- [1] Tinkham M 2004 *Introduction to Superconductivity* (Dover Publications)
- [2] Bauriedl L *et al* 2022 Supercurrent diode effect and magnetochiral anisotropy in few-layer NbSe₂ *Nat. Commun.* **13** 4266
- [3] Sundaresh A, Väyrynen J I, Lyanda-Geller Y and Rokhinson L P 2023 Diamagnetic mechanism of critical current nonreciprocity in multilayered superconductors *Nat. Commun.* **14** 1628
- [4] Lustikova J, Shiomi Y, Yokoi N, Kabeya N, Kimura N, Ienaga K, Kaneko S, Okuma S, Takahashi S and Saitoh E 2018 Vortex rectenna powered by environmental fluctuations *Nat. Commun.* **9** 4922
- [5] Yun J, Son S, Shin J, Park G, Zhang K, Shin Y J, Park J-G and Kim D 2023 Magnetic proximity-induced superconducting diode effect and infinite magnetoresistance in a van der Waals heterostructure *Phys. Rev. Res.* **5** L022064
- [6] Carapella G, Granata V, Russo F and Costabile G 2009 Bistable Abrikosov vortex diode made of a Py–Nb ferromagnet-superconductor bilayer structure *Appl. Phys. Lett.* **94** 242504
- [7] Villegas J E, Savel'ev S, Nori F, Gonzalez E M, Anguita J V, García R and Vicent J L 2003 A superconducting reversible rectifier that controls the motion of magnetic flux quanta *Science* **302** 1188–91
- [8] Chesca B, John D, Pollett R, Gaifullin M, Cox J, Mellor C J and Savel'ev S 2017 Magnetic field tunable vortex diode made of YBa₂Cu₃O_{7– δ} Josephson junction asymmetrical arrays *Appl. Phys. Lett.* **111** 62602
- [9] Jiang K and Hu J 2022 Superconducting diode effects *Nat. Phys.* **18** 1145–6
- [10] Wu H, Wang Y, Xu Y, Sivakumar P K, Pasco C, Filippozzi U, Parkin S S P, Zeng Y-J, McQueen T and Ali M N 2022 The field-free Josephson diode in a van der Waals heterostructure *Nature* **604** 653–6
- [11] Narita H *et al* 2022 Field-free superconducting diode effect in noncentrosymmetric superconductor/ferromagnet multilayers *Nat Nanotechnol* **17** 823–8
- [12] Ando F, Miyasaka Y, Li T, Ishizuka J, Arakawa T, Shiota Y, Moriyama T, Yanase Y and Ono T 2020 Observation of superconducting diode effect *Nature* **584** 373–6
- [13] Lyu -Y-Y *et al* 2021 Superconducting diode effect via conformal-mapped nanoholes *Nat. Commun.* **12** 2703
- [14] Kang K, Berger H, Watanabe K, Taniguchi T, Forró L, Shan J and Mak K F 2022 van der Waals π Josephson junctions *Nano Lett.* **22** 5510–5
- [15] Idzuchi H *et al* 2021 Unconventional supercurrent phase in Ising superconductor Josephson junction with atomically thin magnetic insulator *Nat. Commun.* **12** 5332
- [16] Hou Y *et al* 2023 Ubiquitous superconducting diode effect in superconductor thin films *Phys. Rev. Lett.* **131** 027001
- [17] Vodolazov D Y and Peeters F M 2005 Superconducting rectifier based on the asymmetric surface barrier effect *Phys. Rev. B* **72** 172508
- [18] Hope M K, Amundsen M, Suri D, Moodera J S and Kamra A 2021 Interfacial control of vortex-limited critical current in type-II superconductor films *Phys. Rev. B* **104** 184512
- [19] Simmendinger J, Weigand M, Schütz G and Albrecht J 2020 Magnetic flux penetration into micron-sized superconductor/ferromagnet bilayers *Supercond. Sci. Technol.* **33** 025015
- [20] Nozaki Y, Otani Y, Runge K, Miyajima H, Pannetier B, Nozières J P and Fillion G 1996 Magnetic flux penetration process in two-dimensional superconductor covered with ferromagnetic particle array *J. Appl. Phys.* **79** 8571–7
- [21] Nutting D and Withers F 2021 Flux pinning in NbSe₂–CrGeTe₃ heterostructures *Physica C* **581** 1353803
- [22] Harrington S A, MacManus-Driscoll J L and Durrell J H 2009 Practical vortex diodes from pinning enhanced YBa₂Cu₃O_{7– δ} *Appl. Phys. Lett.* **95** 022518
- [23] Suri D, Kamra A, Meier T N G, Kronseder M, Belzig W, Back C H and Strunk C 2022 Nonreciprocity of vortex-limited critical current in conventional superconducting microbridges *Appl. Phys. Lett.* **121** 102601
- [24] Sobnack M B and Kusmartsev F V 2017 Phase slip avalanches in small superconductors (arXiv:1710.05704)
- [25] Brisbois J *et al* 2016 Imprinting superconducting vortex footsteps in a magnetic layer *Sci. Rep.* **6** 27159
- [26] Novoselov K S, Mishchenko A, Carvalho A and Castro Neto A H 2016 2D materials and van der Waals heterostructures *Science* **353**
- [27] Liu Y, Weiss N O, Duan X, Cheng H-C, Huang Y and Duan X 2016 van der Waals heterostructures and devices *Nat. Rev. Mater.* **1** 16042
- [28] Geim A K and Grigorieva I V 2013 van der Waals heterostructures *Nature* **499** 419–25
- [29] Vlasko-Vlasov V K, Colauto F, Buzdin A I, Rosenmann D, Benseman T and Kwok W-K 2017 Magnetic gates and guides for superconducting vortices *Phys. Rev. B* **95** 144504
- [30] Vlasko-Vlasov V K, Welp U, Imre A, Rosenmann D, Pearson J and Kwok W K 2008 Soft magnetic lithography and giant magnetoresistance in superconducting/ferromagnetic hybrids *Phys. Rev. B* **78** 214511
- [31] El-Bana M S, Wolverson D, Russo S, Balakrishnan G, Paul D M and Bending S J 2013 Superconductivity in two-dimensional NbSe₂ field effect transistors *Supercond. Sci. Technol.* **26** 125020
- [32] Sohn E *et al* 2018 An unusual continuous paramagnetic-limited superconducting phase transition in 2D NbSe₂ *Nat. Mater.* **17** 504–8
- [33] de la Barrera S C *et al* 2018 Tuning Ising superconductivity with layer and spin–orbit coupling in two-dimensional transition-metal dichalcogenides *Nat. Commun.* **9** 1427
- [34] Xi X, Zhao L, Wang Z, Berger H, Forró L, Shan J and Mak K F 2015 Strongly enhanced charge-density-wave order in monolayer NbSe₂ *Nat Nanotechnol* **10** 765–9
- [35] Xi X, Wang Z, Zhao W, Park J-H, Law K T, Berger H, Forró L, Shan J and Mak K F 2016 Ising pairing in superconducting NbSe₂ atomic layers *Nat. Phys.* **12** 139–43
- [36] Li Y F, Wang W, Guo W, Gu C Y, Sun H Y, He L, Zhou J, Gu Z B, Nie Y F and Pan X Q 2018 Electronic structure of ferromagnetic semiconductor CrGeTe₃ by angle-resolved photoemission spectroscopy *Phys. Rev. B* **98** 125127
- [37] Noah A *et al* 2022 Interior and edge magnetization in thin exfoliated CrGeTe₃ films *Nano Lett.* **22** 3165–72
- [38] Han M-G, Garlow J A, Liu Y, Zhang H, Li J, DiMarzio D, Knight M W, Petrovic C, Jariwala D and Zhu Y 2019 Topological magnetic-spin textures in two-dimensional van der Waals Cr₂Ge₂Te₆ *Nano Lett.* **19** 7859–65
- [39] Karapetrov G, Milošević M V, Iavarone M, Fedor J, Belkin A, Novosad V and Peeters F M 2009 Transverse instabilities of multiple vortex chains in magnetically coupled NbSe₂/permalloy superconductor/ferromagnet bilayers *Phys. Rev. B* **80** 180506

- [40] Watson M D *et al* 2020 Direct observation of the energy gain underpinning ferromagnetic superexchange in the electronic structure of CrGeTe₃ *Phys. Rev. B* **101** 205125
- [41] Bawa A, Jha R and Sahoo S 2015 Tailoring phase slip events through magnetic doping in superconductor-ferromagnet composite films *Sci. Rep.* **5** 13459
- [42] Mozaffari S *et al* 2019 Superconducting phase diagram of H₃S under high magnetic fields *Nat. Commun.* **10** 1–6
- [43] Wang Q H *et al* 2022 The magnetic genome of two-dimensional van der Waals materials *ACS Nano* **16** 6960–7079
- [44] He X, Wen Y, Zhang C, Lai Z, Chudnovsky E M and Zhang X 2020 Enhancement of critical current density in a superconducting NbSe₂ step junction *Nanoscale* **12** 12076–82
- [45] Tinkham M, Free J U, Lau C N and Markovic N 2003 Hysteretic I–V curves of superconducting nanowires *Phys. Rev. B* **68** 134515
- [46] Kawarazaki R *et al* 2022 Magnetic-field-induced polarity oscillation of superconducting diode effect *Appl. Phys. Express* **15** 113001
- [47] Gutfreund A *et al* 2023 Direct observation of a superconducting vortex diode *Nat. Commun.* **14** 1630